Symmetry-based calculation of single-particle states and intraband absorption in hexagonal GaN/AlN quantum dot superlattices

Nenad Vukmirović, Zoran Ikonić, Dragan Indjin, and Paul Harrison

School of Electronic and Electrical Engineering, University of Leeds, Leeds LS2 9JT, UK

E-mail: eennv@leeds.ac.uk

Abstract. We present a symmetry based method for the efficient calculation of energy levels in hexagonal GaN/AlN quantum dots within the framework of a $k \cdot p$ model. The envelope functions are expanded into a plane wave basis on a hexagonal lattice and the group projector method is used to adapt the basis to exploit the symmetry, resulting in block diagonalization of the corresponding Hamiltonian matrix into six matrices and classification of the states by the quantum number of total quasi-angular momentum. The method is applied to the calculation of the electron and hole single-particle states in a quantum dot superlattice. The selection rules for absorption of electromagnetic waves in the dipole approximation are established and the intraband optical absorption matrix elements are found. Good agreement with the available experimental data on intraband optical absorption is found.

PACS numbers: 73.21.La, 78.67.Hc

1. Introduction

Wide band-gap III-nitride materials attracted significant research attention in the 1990s which led to the demonstration of commercially attractive emitters in the blue and ultraviolet spectral range [1]. Further improvements in GaN-based optoelectronic devices [2] have been achieved by using GaN quantum dots [3–5] in the active region. GaN quantum dots have also shown to be promising for the realization of solid state quantum computing [6, 7]. In the last few years, intraband transitions in the telecommunication wavelength range (1.3-1.55 μm) in GaN/AlGaN low-dimensional heterostructures at room temperature have been demonstrated [8–11]. Due to ultrafast electron dynamics caused by enhanced interaction with longitudinal optical phonons these transitions can be exploited for realizing detectors and optical modulators operating at high bit-rates. Theoretical proposals also suggest the possibility of operation of GaN quantum well based unipolar devices in the Reststrahlenband ($\sim 34\,\mu$m) where III-As based unipolar devices cannot operate [12, 13].

Having all these possible applications of GaN quantum dots in mind, there have been several theoretical studies of their electronic structure [14–19]. The energy levels of GaN/AlGaN hexagonal quantum dots taking into account strain distribution as well as internal electric fields generated due to spontaneous and piezoelectric polarization were calculated in [14] using the plane wave expansion method within the framework of the $k \cdot p$ model and in [15] and [16] using the tight-binding approach. Spherical unstrained GaN quantum dots have also been studied theoretically [17,18]. In our recent work [20], symmetry considerations were used in modelling the square-based pyramidal InAs/GaAs quantum dots. However, although the electronic states in III-nitride dots have been symmetry classified in [21], the hexagonal symmetry of the dots hasn't yet been exploited in the calculation of the single-particle states. So far, the intraband absorption in III-nitride quantum dots was treated within the simple quantum well approach only [10]. No theoretical studies of intraband absorption taking into account a fully three dimensional nature of electron confinement have been reported.

Along this line, the aim of this paper is to exploit the symmetry in the calculation of energy levels of hexagonally shaped GaN/AlN quantum dots within the framework of $k \cdot p$ method and apply the developed symmetry based method to study intraband transitions in these dots theoretically. We start by briefly reviewing the theoretical framework in section 2 and in section 3 we show how symmetry can be exploited in the calculation of energy levels and intraband absorption. The results obtained are presented in section 4.

2. Theoretical framework

The 8-band $k \cdot p$ Hamiltonian for semiconductors with wurtzite crystal structure [22] can be block diagonalized into two 4-band Hamiltonians for carriers with opposite values of spin assuming the spin-orbit splitting Δ_{so} is zero (such an approximation is justified by

its small value in nitrogen containing semiconductors $\Delta_2 = \Delta_{so}/3 \lesssim 5\,\mathrm{meV}$ [23]). The state of the electron is then of the form

$$|\Psi\rangle = \sum_{l=1}^{4} \psi_l(\boldsymbol{r})|l\rangle, \tag{1}$$

where $\psi_l(\boldsymbol{r})$ are the slowly varying envelope functions of electron states ($l = 1$), heavy hole states ($l = 2$ and $l = 3$), and light hole states ($l = 4$), and $|l\rangle$ the corresponding Bloch functions

$$\begin{aligned} |1\rangle &= |S\uparrow\rangle, \\ |2\rangle &= \frac{1}{\sqrt{2}}|(X + iY)\uparrow\rangle, \\ |3\rangle &= \frac{1}{\sqrt{2}}|(X - iY)\uparrow\rangle, \\ |4\rangle &= |Z\uparrow\rangle. \end{aligned} \tag{2}$$

The 4-band Hamiltonian is of the form

$$\hat{H} = \hat{H}_k + \hat{H}_s + V_p I_4, \tag{3}$$

where $\hat{H}_k$ is the kinetic part of the Hamiltonian, $\hat{H}_s$ the strain part, V_p the potential induced due to spontaneous and piezoelectric polarizations present in III-nitride materials [24] and I_4 the 4×4 unity matrix. The explicit expressions for $\hat{H}_k$ and $\hat{H}_s$ can be found in [14] and [22].

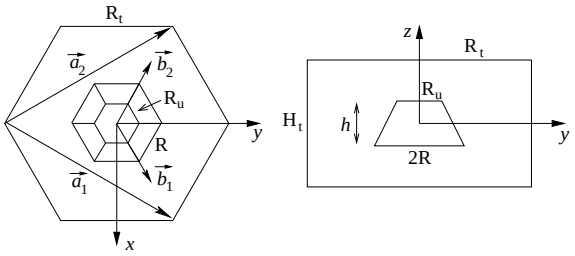

Figure 1. Schematic view of a truncated hexagonal pyramid quantum dot with upper base radius R_u, lower base radius R and height h embedded in a hexagonal prism with radius R_t and height H_t – top view (left) and side view (right). The primitive vectors of the corresponding Bravais lattice ($\boldsymbol{a}_1$ and $\boldsymbol{a}_2$) and its reciprocal lattice ($\boldsymbol{b}_1$ and $\boldsymbol{b}_2$) are also shown in the figure.

In the plane wave expansion method [20, 25–30] the envelope functions are assumed as a linear combination of plane waves with the coefficients in the expansion to be determined. Conventionally, the dot is embedded in a rectangular box and the plane waves that form the basis of functions periodic on a cubic lattice are taken. However, in this work, due to the hexagonal shape of the dots, it seems more natural to embed the dot in a hexagonal prism and take the plane waves that form the basis of functions

periodic on a hexagonal lattice in the expansion. Let the dot be embedded in a hexagonal prism with side length R_t and height H_t, as shown in figure 1. The primitive vectors of the Bravais lattice corresponding to the hexagonal lattice are given by

$$\begin{aligned}\boldsymbol{a}_1 &= R_t\left(\frac{\sqrt{3}}{2}\boldsymbol{e}_x + \frac{3}{2}\boldsymbol{e}_y\right),\\ \boldsymbol{a}_2 &= R_t\left(\frac{-\sqrt{3}}{2}\boldsymbol{e}_x + \frac{3}{2}\boldsymbol{e}_y\right),\\ \boldsymbol{a}_3 &= H_t\boldsymbol{e}_z.\end{aligned} \tag{4}$$

The primitive vectors of the reciprocal lattice $\boldsymbol{b}_j$ $(j = 1, 2, 3)$ satisfy the condition $\boldsymbol{a}_i \cdot \boldsymbol{b}_j = 2\pi\delta_{ij}$ and are therefore given by

$$\begin{aligned}\boldsymbol{b}_1 &= \frac{4\pi}{3R_t}\left(\frac{\sqrt{3}}{2}\boldsymbol{e}_x + \frac{1}{2}\boldsymbol{e}_y\right),\\ \boldsymbol{b}_2 &= \frac{4\pi}{3R_t}\left(-\frac{\sqrt{3}}{2}\boldsymbol{e}_x + \frac{1}{2}\boldsymbol{e}_y\right),\\ \boldsymbol{b}_3 &= \frac{2\pi}{H_t}\boldsymbol{e}_z.\end{aligned} \tag{5}$$

The envelope functions are then assumed in the form

$$\psi_l(\boldsymbol{r}) = \sum_{\boldsymbol{k}} A_{l,\boldsymbol{k}} e^{i\boldsymbol{k}\cdot\boldsymbol{r}}, \tag{6}$$

where the summation is performed over $\boldsymbol{k}$ vectors given by

$$\boldsymbol{k} = m_1\boldsymbol{b}_1 + m_2\boldsymbol{b}_2 + m_3\boldsymbol{b}_3, \tag{7}$$

where $m_1 \in \{-n_1, \ldots, n_1\}$, $m_2 \in \{-n_2, \ldots, n_2\}$, $m_3 \in \{-n_3, \ldots, n_3\}$, where $n_1 = n_2$ and n_3 are positive integers. After putting (6) into the Hamiltonian eigenvalue problem

$$\sum_{j=1}^{4} H_{ij}\psi_j(\boldsymbol{r}) = E\psi_i(\boldsymbol{r}) \tag{8}$$

one arrives at the eigenvalue problem of the Hamiltonian matrix

$$\sum_{j,\boldsymbol{k}} h_{ij}(\boldsymbol{q}, \boldsymbol{k}) A_{j,\boldsymbol{k}} = E A_{i,\boldsymbol{q}}, \tag{9}$$

where

$$h_{ij}(\boldsymbol{q}, \boldsymbol{k}) = \frac{1}{V}\int_V \mathrm{d}^3\boldsymbol{r} \exp\left(-i\boldsymbol{q}\cdot\boldsymbol{r}\right) H_{ij} \exp\left(i\boldsymbol{k}\cdot\boldsymbol{r}\right) \tag{10}$$

are the Hamiltonian matrix elements (the integration is performed over the volume of the hexagonal unit cell).

All the elements of the kinetic part of the Hamiltonian are linear combination of terms of the form $E_1 = P(\boldsymbol{r})$, $E_2 = P(\boldsymbol{r})k_ik_j$ or $E_3 = P(\boldsymbol{r})k_i$, where $k_i = -i\frac{\partial}{\partial x_i}$,

($i = x, y, z$) are differential operators, and therefore the corresponding elements of the Hamiltonian matrix are given by linear combination of terms of the form

$$\begin{aligned} E_1(\boldsymbol{q},\boldsymbol{k}) &= P^M\delta_{\boldsymbol{q},\boldsymbol{k}} - \frac{(2\pi)^3}{V}\Delta P\chi(\boldsymbol{q}-\boldsymbol{k}), \\ E_2(\boldsymbol{q},\boldsymbol{k}) &= \frac{1}{2}\left(k_iq_j + q_ik_j\right)\left[P^M\delta_{\boldsymbol{q},\boldsymbol{k}} - \frac{(2\pi)^3}{V}\Delta P\chi(\boldsymbol{q}-\boldsymbol{k})\right], \\ E_3(\boldsymbol{q},\boldsymbol{k}) &= \frac{1}{2}\left(k_i+q_i\right)\left[P^M\delta_{\boldsymbol{q},\boldsymbol{k}} - \frac{(2\pi)^3}{V}\Delta P\chi(\boldsymbol{q}-\boldsymbol{k})\right], \end{aligned} \tag{11}$$

where P^M is the value of the material parameter P in the matrix material, $\Delta P = P^M - P^{QD}$ is the difference between its values in the matrix and the quantum dot, and $\chi(\boldsymbol{q})$ is the Fourier transform of the quantum dot characteristic function defined as

$$\chi(\boldsymbol{q}) = \frac{1}{(2\pi)^3}\int_{\mathrm{QD}} \mathrm{d}^3\boldsymbol{r}\exp\left(-i\boldsymbol{q}\cdot\boldsymbol{r}\right), \tag{12}$$

where the integration is performed over the volume of the quantum dot (QD) only. It can be calculated analytically in terms of the geometrical parameters of the dot. The same recipe for the order of differential and multiplication operators in the Hamiltonian as in [20] was taken.

All the elements of the strain part of the Hamiltonian are linear combinations of terms of the form $E_4 = P(\boldsymbol{r})e_{jk}$ (where e_{jk} are the strain tensor components) and therefore the corresponding Hamiltonian matrix elements are linear combinations of terms of the form

$$E_4(\boldsymbol{q},\boldsymbol{k}) = \frac{(2\pi)^3}{V}P^M e_{jk}(\boldsymbol{q}-\boldsymbol{k}) - \frac{(2\pi)^6}{V^2}\Delta P\sum_{\boldsymbol{q}'}\chi(\boldsymbol{q}-\boldsymbol{k}-\boldsymbol{q}')e_{jk}(\boldsymbol{q}'), \tag{13}$$

where

$$e_{ij}(\boldsymbol{q}) = \frac{1}{(2\pi)^3}\int_V \mathrm{d}^3\boldsymbol{r}\exp\left(-i\boldsymbol{q}\cdot\boldsymbol{r}\right)e_{ij}(\boldsymbol{r}), \tag{14}$$

are Fourier transforms of the strain tensor components that can be calculated from the analytical formulae given in [14].

The elements of the Hamiltonian matrix due to the presence of spontaneous and piezoelectric polarization are given by [14]

$$h^p_{ij}(\boldsymbol{q},\boldsymbol{k}) = \frac{(2\pi)^3}{V}\frac{ie}{(\boldsymbol{q}-\boldsymbol{k})^2\varepsilon_0\varepsilon_r}(\boldsymbol{q}-\boldsymbol{k})\cdot\boldsymbol{P}(\boldsymbol{q}-\boldsymbol{k})\delta_{ij}, \tag{15}$$

where ε_0 is the vacuum dielectric constant, ε_r the static dielectric constant, e the magnitude of the elementary charge and $\boldsymbol{P}(\boldsymbol{q})$ is the Fourier transform of the sum of the spontaneous and piezoelectric polarization vectors $\boldsymbol{P} = \boldsymbol{P}^{sp} + \boldsymbol{P}^{pz}$. The spontaneous polarization vector is given by $\boldsymbol{P}^{sp} = P^{sp}\boldsymbol{e}_z$, while the piezoelectric polarization components are related to strain tensor components by [29, 31]

$$\begin{aligned} P^{pz}_1 &= 2\epsilon_{15}e_{13}, \\ P^{pz}_2 &= 2\epsilon_{15}e_{23}, \\ P^{pz}_3 &= \epsilon_{31}(e_{11}+e_{22}) + \epsilon_{33}e_{33}, \end{aligned} \tag{16}$$

where ϵ_{ij} are the piezoelectric constants. The Fourier transform $\boldsymbol{P}(\boldsymbol{q})$ can therefore be calculated in a similar way as the kinetic and strain Hamiltonian matrix elements.

The Hamiltonian $\hat{H}'$ of the interaction with the electromagnetic field is obtained by replacing $\boldsymbol{k}$ with $\boldsymbol{k}+\frac{e}{\hbar}\boldsymbol{A}$ in the kinetic part $\hat{H}_k$ of the $k\cdot p$ Hamiltonian [32] (where $\boldsymbol{A}=A\,\boldsymbol{\varepsilon}$ is the magnetic vector potential, $\boldsymbol{\varepsilon}$ is the polarization vector of the radiation and $\hbar$ the reduced Planck's constant), i.e. $\hat{H}'=\hat{H}_k(\boldsymbol{k}+\frac{e}{\hbar}\boldsymbol{A})-\hat{H}_k(\boldsymbol{k})$. In the dipole approximation $\boldsymbol{A}$ is considered constant in space, and furthermore all the terms quadratic in $\boldsymbol{A}$ are neglected. The optical cross section of the $i\to f$ transition due to absorption of electromagnetic radiation of angular frequency ω is given by [33]

$$\sigma_{if}^{\boldsymbol{\varepsilon}}(\omega)=\frac{2\pi}{\overline{n}\varepsilon_0 c\omega}\left|\mathcal{M}_{if}^{\boldsymbol{\varepsilon}}\right|^2 g(E_f-E_i-\hbar\omega,2\sigma). \tag{17}$$

where $\overline{n}$ is the refraction index, c the speed of light in vacuum, and E_f and E_i are the energies of the final and the initial state, respectively. $\mathcal{M}_{if}^{\boldsymbol{\varepsilon}}=\left\langle i\left|\hat{H}'\right|f\right\rangle/A$ is the matrix element which depends only on the direction $\boldsymbol{\varepsilon}$ of light polarization and not on the amplitude of A. The inhomogeneous broadening due to size inhomogeneity of the quantum dot ensemble was taken into account by replacing the delta function in Fermi's golden rule, with a Gaussian given by

$$g(x,2\sigma)=\frac{1}{\sigma\sqrt{2\pi}}\exp\left(-\frac{x^2}{2\sigma^2}\right). \tag{18}$$

The matrix element is equal to

$$\mathcal{M}_{if}^{\boldsymbol{\varepsilon}}=V\sum_{l,\boldsymbol{q}}\sum_{j,\boldsymbol{k}}A_{l,\boldsymbol{q}}^{i*}A_{j,\boldsymbol{k}}^{f}G_{lj}(\boldsymbol{q},\boldsymbol{k}), \tag{19}$$

where V is the volume of the embedding hexagonal prism and

$$G_{lj}(\boldsymbol{q},\boldsymbol{k})=\frac{1}{AV}\int_V \mathrm{d}^3\boldsymbol{r}\exp\left(-i\boldsymbol{q}\cdot\boldsymbol{r}\right)H'_{lj}\exp\left(i\boldsymbol{k}\cdot\boldsymbol{r}\right) \tag{20}$$

are the Fourier transforms of the perturbation Hamiltonian matrix elements that can all be calculated analytically, as well.

3. Symmetry considerations

The symmetry of the hexagonal quantum dot system when the location of every atom is taken into account is C_{3v} and is lower than the symmetry of the dot geometrical shape [21, 34]. When the dot dimensions are large compared with the unit cell, $k\cdot p$ method is considered to be a reliable tool for calculating the electronic structure of semiconductor heterostructures. The symmetry of the $k\cdot p$ model itself is equal to the symmetry of the wurtzite crystal lattice, which is given by the C_{6v}^4 space group [21,35]. The symmetry of the kinetic part of the $k\cdot p$ Hamiltonian applied to quantum dots is equal to the intersection of the C_{6v} symmetry of the dot geometrical shape and the C_{6v}^4 symmetry of wurtzite crystal lattice, and is represented by the C_{6v} group. The strain part of the Hamiltonian doesn't break that symmetry when the strain distribution is taken into account via the continuum mechanical model [36], as is done here. The

spontaneous polarization is directed along $z-$axis and obviously preserves the symmetry. In contrast to square based pyramidal InAs/GaAs quantum dots, where piezoelectric effects reduce the symmetry [20] from C_{4v} to C_{2v}, the piezoelectric potential in the dots considered here is C_{6v} symmetric and doesn't affect the symmetry of the Hamiltonian. Consequently, the symmetry of the Hamiltonian is C_{6v}. In this work, only the C_6 symmetry will be exploited as the presence of an external axial magnetic field reduces the symmetry from C_{6v} to C_6, and although we do not consider the magnetic field effects in this paper, the derived symmetry adapted basis is general enough to be used in such situations as well.

The 4-band Hamiltonian (3) commutes with the rotations around the z-axis by $\varphi_k = k \cdot 2\pi/6$ ($k \in \{0, 1, \ldots, 11\}$) which are generated by the operator of $z-$component of the total angular momentum $\hat{F}_z$, which is a sum of orbital angular momentum of the envelope function $\hat{L}_z$ and total angular momentum of the Bloch function $\hat{J}_z$. The action of the generator of the double valued representation of the rotation group

$$\hat{D}(R_{\varphi_1}) = e^{-i\hat{F}_z\varphi_1} \tag{21}$$

on the basis vectors of Hilbert space

$$|\boldsymbol{k}, i\rangle = e^{i\boldsymbol{k}\cdot\boldsymbol{r}}|i\rangle, \tag{22}$$

(where $\boldsymbol{k}$ vectors are given by (7) and $i \in \{1, 2, 3, 4\}$) is given by

$$\hat{D}(R_{\varphi_1})|\boldsymbol{k}, i\rangle = e^{i\boldsymbol{k}'\cdot\boldsymbol{r}}e^{-iJ_z(i)\varphi_1}|i\rangle, \tag{23}$$

where $J_z(1) = 1/2$, $J_z(2) = 3/2$, $J_z(3) = -1/2$, $J_z(4) = 1/2$ and the $\boldsymbol{k}$-vector is rotated by φ_1 around the $z-$axis

$$\boldsymbol{k}' = R_{\varphi_1}\boldsymbol{k} = (m_1 - m_2)\boldsymbol{b}_1 + m_1\boldsymbol{b}_2 + m_3\boldsymbol{b}_3, \tag{24}$$

or in the Descartes coordinates

$$\begin{aligned} k'_x + ik'_y &= e^{i\varphi_1}(k_x + ik_y), \\ k'_z &= k_z. \end{aligned} \tag{25}$$

The orbit of action of the group elements on the basis vectors when $(m_1, m_2) = (0, 0)$ is a one-dimensional space $\mathcal{H}_{(0,0,m_3),i}$. The introduced labelling of the form $(m_1, m_2, m_3), i$ will also be used in the rest of the text to label the reduction of representation $\hat{D}$ to the space $\mathcal{H}_{(m_1,m_2,m_3),i}$, as well as to label the group projectors and the elements of the symmetry adapted basis belonging to this space. In $\mathcal{H}_{(0,0,m_3),i}$ the representation $\hat{D}$ reduces to

$$\hat{D}_{(0,0,m_3),i}(R_{\varphi_1}) = e^{-iJ_z(i)\varphi_1}. \tag{26}$$

On the other hand, when $(m_1, m_2) \neq (0, 0)$ the orbit is a 6-dimensional space $\mathcal{H}_{(m_1,m_2,m_3),i}$ (with $0 \leq m_2 < m_1$ to avoid multiple counting of the same space) spanned by the vectors $|bl\rangle = |R_{l\varphi_1}\boldsymbol{k}, i\rangle$ ($l \in \{0, 1, \ldots, 5\}$). The operator $\hat{D}(R_{\varphi_1})$ in this basis reads

$$\hat{D}_{(m_1,m_2,m_3),i}(R_{\varphi_1}) = e^{-iJ_z(i)\varphi_1} \begin{bmatrix} 0 & 1 \\ I_5 & 0 \end{bmatrix}, \tag{27}$$

where I_5 is the 5×5 unity matrix. The characters of the group elements in this representation are then given by

$$\chi(\hat{D}_{(m_1,m_2,m_3),i}(R_{l\varphi_1})) = 6\delta_{l,0} - 6\delta_{l,6} \tag{28}$$

and

$$\chi(\hat{D}_{(0,0,m_3),i}(R_{l\varphi_1})) = e^{-iJ_z(i)l\varphi_1}. \tag{29}$$

Consequently one finds the reduction of the representation in these spaces to its irreducible double valued representations A_{m_f} whose characters are given by $\chi\left(A_{m_f}(R_{l\varphi_1})\right) = \exp(-ilm_f\varphi_1)$ (where $m_f \in \{-5/2, -2, -3/2, \ldots, 5/2\}$ and $l \in \{0, 1, \ldots, 11\}$):

$$\hat{D}_{(0,0,m_3),i} = A_{J_z(i)} \tag{30}$$

and

$$\hat{D}_{(m_1,m_2,m_3),i} = A_{-5/2} + A_{-3/2} + A_{-1/2} + A_{1/2} + A_{3/2} + A_{5/2}. \tag{31}$$

From (30) and (31), one gets that the reduction of $\hat{D}$ to the irreducible representations is given by

$$\hat{D} = N_{-5/2}A_{-5/2}+N_{-3/2}A_{-3/2}+N_{-1/2}A_{-1/2}+N_{1/2}A_{1/2}+N_{3/2}A_{3/2}+N_{5/2}A_{5/2}, \tag{32}$$

where $N_{1/2} = 6n_3\left[2 + 2n_1(n_1+1)\right]$, $N_{-1/2} = N_{3/2} = 6n_3\left[1 + 2n_1(n_1+1)\right]$ and $N_{-3/2} = N_{5/2} = N_{-5/2} = 12n_3n_1(n_1+1)$. The projection operators [37] are given by

$$\hat{P}_{A_{m_f}}((0,0,m_3),i) = 1 \tag{33}$$

and

$$\hat{P}_{A_{m_f}}((m_1,m_2,m_3),i) = \frac{1}{12}\sum_{l=0}^{11} \chi\left(A_{m_f}(R_{l\varphi_1})\right)^* \hat{D}_{(m_1,m_2,m_3),i}(R_{l\varphi_1}). \tag{34}$$

After explicit calculation one gets

$$\hat{P}_{A_{m_f}}((m_1,m_2,m_3),i) = M(e^{i\varphi_1(J_z(i)-m_f)}), \tag{35}$$

where $M(u)$ is the matrix defined by

$$M(u) = \begin{bmatrix} 1 & u & u^2 & u^3 & u^4 & u^5 \\ u^5 & 1 & u & u^2 & u^3 & u^4 \\ u^4 & u^5 & 1 & u & u^2 & u^3 \\ u^3 & u^4 & u^5 & 1 & u & u^2 \\ u^2 & u^3 & u^4 & u^5 & 1 & u \\ u & u^2 & u^3 & u^4 & u^5 & 1 \end{bmatrix}. \tag{36}$$

The elements of the symmetry adapted basis are finally given by

$$\begin{aligned} &|A_{1/2},(0,0,m_3),1\rangle = |(0,0,m_3),1\rangle, \\ &|A_{3/2},(0,0,m_3),2\rangle = |(0,0,m_3),2\rangle, \\ &|A_{-1/2},(0,0,m_3),3\rangle = |(0,0,m_3),3\rangle, \\ &|A_{1/2},(0,0,m_3),4\rangle = |(0,0,m_3),4\rangle, \end{aligned} \tag{37}$$

where $-n_3 \leq m_3 \leq n_3$ and

$$|A_{m_f}, (m_1, m_2, m_3), i\rangle = \frac{1}{\sqrt{6}} \sum_{l=0}^{5} e^{il\varphi_1(m_f - J_z(i))} |bl\rangle, \tag{38}$$

where $0 \leq m_2 < m_1 \leq n_1 = n_2$, $-n_3 \leq m_3 \leq n_3$, $i \in \{1, 2, 3, 4\}$ and $m_f \in \{-5/2, -3/2, -1/2, 1/2, 3/2, 5/2\}$.

In this basis, the Hamiltonian matrix is block diagonal with 6 blocks of approximately equal size (More precisely, the sizes of the blocks are $N_{1/2}$, $N_{-1/2} = N_{3/2}$ and $N_{-3/2} = N_{5/2} = N_{-5/2}$, see equation 32). Since all the elements of the symmetry adapted basis are linear combinations of the elements of the plane wave basis, all the elements of the 6 blocks of the Hamiltonian matrix can be expressed in terms of the elements of the Hamiltonian matrix in the plane wave basis. The computational time necessary to diagonalize 6 blocks is approximately 36 times smaller than the time necessary within the straightforward plane-wave approach.

Apart from reducing the computational time within the plane wave method, the method presented introduces the quantum number m_f which can be interpreted as the total quasi-angular momentum. The selection rules for the interaction with electromagnetic radiation in the dipole approximation have then been derived as: $\Delta m_f = 0$ for $z-$polarized light and $\Delta m_f = \pm 1$ for in-plane polarized light (where by the definition $5/2 + 1 = -5/2$ and $-5/2 - 1 = 5/2$). These rules are very restrictive, and although the quantum dots allow for the absorption of radiation of any polarization in contrast to quantum wells, these transitions are allowed only for certain pairs of states.

In the rest of the paper, based on the symmetry classification discussed, we label the states in the conduction band using the following notation: ne_{m_f} represents the n-th electron state (in ascending order of energies) among the states having quantum number m_f.

4. Results

The method presented was first applied to the calculation of electron and hole energy levels in an ideally periodic array of hexagonal truncated pyramidal GaN/AlN quantum dots. In a realistic case the number of quantum dot layers is finite and therefore the strain distribution and the effective potential are not strictly periodic. It is also difficult to achieve identical size of the dots in all layers. Nevertheless, in a quantum dot superlattice containing several tens of quantum dot layers one certainly expects that the results obtained within the periodic model can be used as a very good approximation of the actual system. The dot radius was taken to be $R = 9.0\,\text{nm}$, the height $h = 3.7\,\text{nm}$, the upper base radius $R_u = 3.5\,\text{nm}$ and the diameter of the embedding box $2R_t = 15.0\,\text{nm}$. The period of the superlattice was varied over the interval from $H_t = 4.3\,\text{nm}$, when the dots almost lie on top of one another, to $H_t = 12.3\,\text{nm}$. Material parameters in the calculation were taken from [23]. The unstrained AlN conduction

band edge was taken as the reference level. The number of plane waves used in the calculation was $n_1 = n_2 = 12$ and $n_3 = 10$ and chosen to ensure convergence to better than 1 meV for the ground state in the conduction band and the convergence of the order of 1 meV for those excited states in the conduction band that are mainly responsible for the absorption of $z-$polarized radiation.

The effective electron potential on the z-axis defined as $V_e = H_{11}(k = 0)$, the heavy hole potential defined as $V_{hh} = H_{22}(k = 0)$, and the light hole potential defined as $V_{lh} = H_{44}(k = 0)$ are shown in figures 2 and 3. One can see that significant changes in the effective potentials occur when varying the period of the structure, which therefore influence considerably the electronic structure of the quantum dot superlattice.

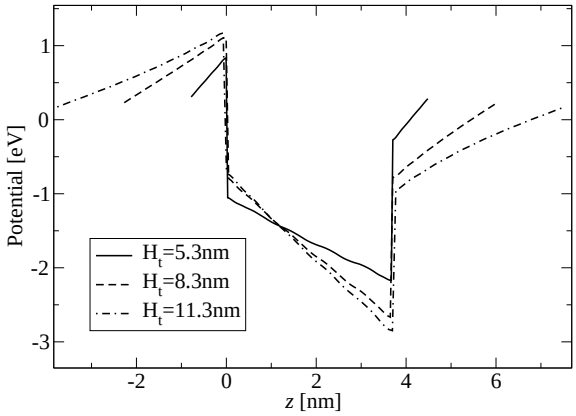

Figure 2. The effective potential on the z-axis experienced by electrons for three different values of the period H_t.

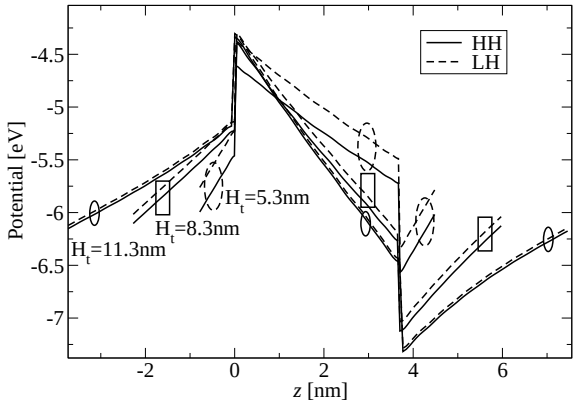

Figure 3. The effective potential on the z-axis experienced by light (LH) and heavy holes (HH) for three different values of the period H_t.

The electron and hole energy levels, when the period is varied in the above interval, are shown in figure 4. For each value of m_f, the first few energy levels in the conduction band and the highest energy level in the valence band are shown. A very weak dispersion with the superlattice Bloch wave vector K_z was found and therefore only $K_z = 0$ states are presented. To illustrate this effect, the wave functions of the electron and hole ground states when the period is equal to $H_t = 5.3\,\mathrm{nm}$ are shown in figure 5. One can see that there is no overlap between the states of neighboring periods and hence no electronic coupling. Therefore, even in the case of dots that almost lie on top each other, electronic coupling is almost negligible. The origin of such a weak electronic coupling between dots in a superlattice is the strong internal electric field (see figures 2 and 3) that creates a deep triangular potential well at the top of the dot for electrons (and at the bottom of the dot for holes) which prevents interaction between neighboring dots. Another effect caused by the electric field that can be also verified from figure 5 is the localization of the electron states at the top of the dot and hole states at the bottom of the dot, as previously reported by others [14, 38].

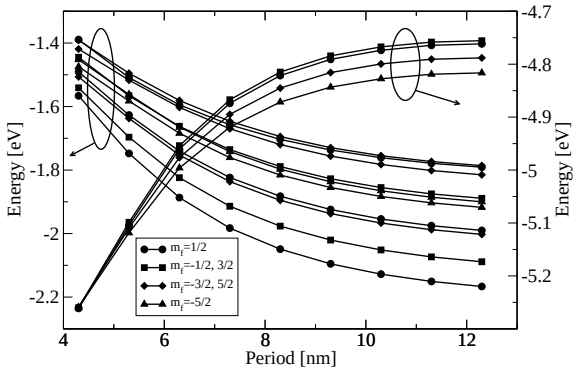

Figure 4. The dependence of electron (left axis) and hole (right axis) energy levels on the superlattice period. For each value of m_f, the first few energy levels in the conduction band and the highest energy level in the valence band are shown.

The energy levels with $m_f = -1/2$ and $m_f = 3/2$ are degenerate. The same holds for $m_f = -3/2$ and $m_f = 5/2$. The origin of these degeneracies is the fact that the used 4-band Hamiltonian also commutes with the operators of rotations and reflections in *real* space, that form the single valued representation of the C_{6v} group. The mentioned degeneracy then stems from two dimensional irreducible representations of the C_{6v} group.

One can see from figure 4 that as the superlattice period increases, the effective energy gap of the structure decreases, in contrast to the behavior observed in InAs/GaAs. Such a behavior is governed by the changes in the value of the internal electric field. As the distance between the dots increases, the field in the dot also becomes larger, the effective electron and hole potential wells are therefore deeper (figures 2 and 3)

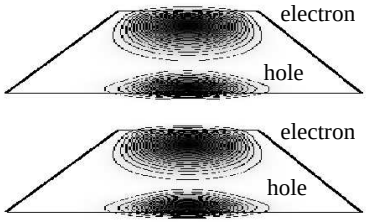

Figure 5. Wave functions moduli squared in the yz-plane of the electron and hole ground states when the period is equal to $H_t = 5.3\,\mathrm{nm}$.

and consequently both electron and hole states are more confined.

We further discuss the type of hole states: When the superlattice period is small ($H_t \sim 5\,\mathrm{nm}$), the effective potential for light holes is significantly larger than for heavy holes (figure 3) and despite the smaller light hole effective mass, they are more strongly confined and therefore the hole ground state is of light hole type. However, when the period increases, the difference between the light and heavy hole effective potentials becomes smaller, and due to the larger effective mass, the hole ground state becomes of the heavy hole type. In the intermediate region, we find that the ground hole state is a mixed light and heavy hole state. However, this region is very narrow and although interesting effects in the optical spectrum due to hole mixing can be expected, it would be very hard to access this region experimentally. As far as excited hole states are concerned, due to the above mentioned effects, when the period increases the heavy hole character of the states also prevails.

As the ground electron state has $m_f = 1/2$ and selection rules for the absorption of $z-$polarized radiation only allow the transitions with $\Delta m_f = 0$, it follows that the peak positions in the $z-$polarized radiation absorption spectrum will be determined by the positions of the energy levels having $m_f = 1/2$ symmetry. The dependence of the positions of the $m_f = 1/2$ energy levels on the period of the structure is given in figure 6. One can see that the first three well separated energy levels (labeled as 1, 2 and 3) are followed by three groups of closely spaced levels (labeled as G1, G2 and G3).

Although the symmetry allows transitions from the ground state to any of the $m_f = 1/2$ states, it turns out that only some of these transitions have significant values of matrix elements. The intraband optical absorption spectrum from the ground state for $z-$polarized radiation is shown in figure 7. The standard deviation σ of the Gaussian linewidth on each of the transitions was taken to be equal to 10% of the transition energy, which is approximately the experimental value in [10]. The strongest absorption occurs for the transition from the ground state to the states from the G1 group, as the matrix elements for these transitions are the largest, figure 8 (among them the strongest is the transition to $4e_{1/2}$). The absorption maximum at $H_t = 8.3\,\mathrm{nm}$ occurs at 490 meV, and is followed by a weaker line with a maximum at 860 meV originating from the

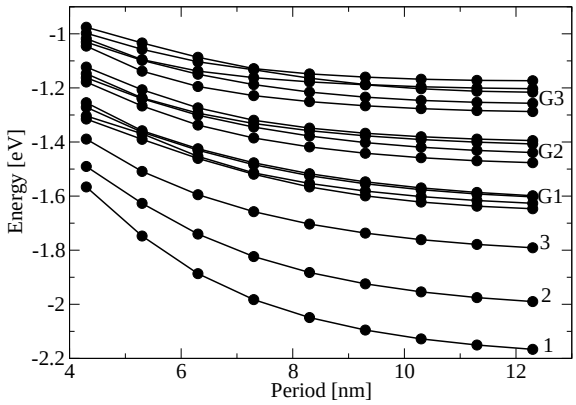

Figure 6. The dependence of the $m_f = 1/2$ electron energy levels on the period of the structure.

transitions to the G3 group of states. These results are in reasonable agreement with the experimental results of [10], where for the same value of the period and for dots of similar size the strongest absorption occurs at 520 meV or 590 meV for two different samples investigated there, and is followed by two weaker lines at 730 meV and 980 meV or 850 meV and 970 meV.

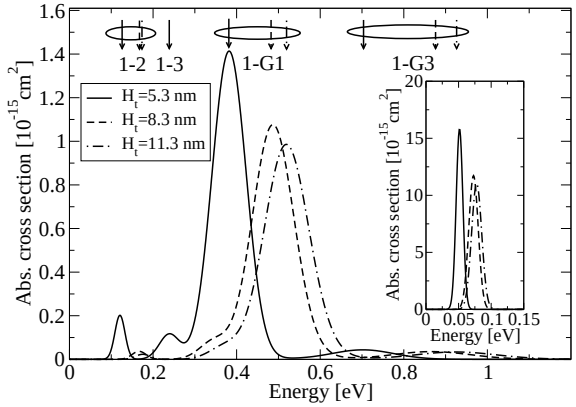

Figure 7. Intraband optical absorption spectrum from the ground state for $z-$polarized radiation for three different values of the structure period. The corresponding spectrum for $x-$polarized radiation is shown in the inset.

The wave functions of the first four states with $m_f = 1/2$ are shown in figure 9. The absorption of $z-$polarized radiation from $1e_{1/2}$ is strongest towards $4e_{1/2}$, although both $2e_{1/2}$ and $3e_{1/2}$ have excellent spatial overlap with $1e_{1/2}$ as well. In order to explain why the absorption matrix element is much larger on the $1e_{1/2} \rightarrow 4e_{1/2}$ transition, one may notice that the states $1e_{1/2} - 3e_{1/2}$ are nearly symmetric with respect to reflections

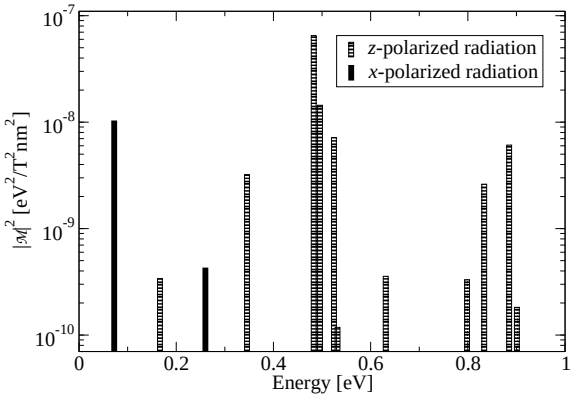

Figure 8. Optical absorption matrix elements $|\mathcal{M}|^2$ vs. energy for different intraband transitions from the ground state to excited states when the period is equal H_t = 8.3 nm.

through the plane normal to the $z-$axis, denoted in figure 9 by a dashed line. If that symmetry was exact, the transitions between those states due to the interaction with $z-$polarized radiation would be strictly forbidden, but since it is only approximate the matrix elements of those transitions have relatively small values. As seen from figure 9, the state $4e_{1/2}$ is asymmetric with respect to the mentioned plane and its spatial overlap with the ground state is still good, therefore the strongest absorption occurs for the $1e_{1/2} \rightarrow 4e_{1/2}$ transition.

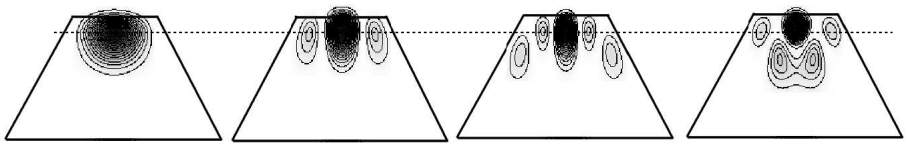

Figure 9. Wave function moduli squared in the yz-plane of the first four electron states with $m_f = 1/2$ when the period is equal to H_t = 8.3 nm. The states $1e_{1/2}$, $2e_{1/2}$, $3e_{1/2}$ and $4e_{1/2}$ are shown respectively from left to right.

The optical cross section for the absorption of $x-$polarized radiation from the ground state is shown in the inset of figure 7. Symmetry imposed selection rules generally allow transitions to any state having $m_f = -1/2$ or $m_f = 3/2$, but in reality the spectrum is entirely dominated by the transition from the ground state (having $m_f = 1/2$) to the degenerate pair of first excited states (having m_f=$-1/2$, $3/2$). The wave functions of the $1e_{1/2}$ and $1e_{-1/2,3/2}$ states are presented in figure 10. The spatial overlap is good and there are no approximate selection rules that would inhibit the transition between these states as in the previous case. The transitions to higher states

contribute much less to the absorption due to a reduced spatial overlap with the ground state resulting in smaller matrix elements (figure 8) and an increased transition energy. As the dot shape investigated is not cylindrical but hexagonal, the absorption of in-plane polarized radiation should in principle depend on the polarization vector. However, we have found that the change of absorption for different directions of the polarization vector in the $xy-$plane is less than 1% and therefore the results shown in the inset of figure 7 are valid for any direction of in-plane polarized radiation.

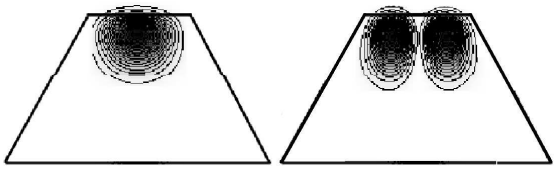

Figure 10. Wave function moduli squared in the yz-plane of the $1e_{1/2}$ (left) and $1e_{-1/2,3/2}$ (right) states.

5. Conclusion

In conclusion, a symmetry based method for the calculation of single particle states in hexagonal GaN/AlN quantum dots within the framework of the $k \cdot p$ model has been developed. The method has been applied to calculate the electron and hole states in a quantum dot superlattice. It has been found that the changes in the electronic structure when the period of the structure is varied are caused by changes in the internal electric field and not by the electronic coupling which was found to be negligible. The changes in strain distribution mainly determine the type of hole states. Furthermore, intraband absorption in the conduction band was studied. Selection rules for interaction with electromagnetic radiation were derived and the absorption spectra from the ground state for different polarizations of incident radiation were calculated. The absorption spectrum for in-plane polarized light is dominated by the transition to two degenerate first excited states, while for $z-$polarized light it is determined by the absorption to a group of excited states located $\sim 500\,\mathrm{meV}$ above the ground state having the same symmetry as the ground state. Such result is in overall agreement with the available experimental data on intraband absorption in the conduction band in GaN/AlN quantum dots.

References

[1] Nakamura S and Fasol G 1997 *The Blue Laser Diode* (Springer, Berlin)
[2] Arakawava Y 2002 *IEEE J. Select. Topics Quantum Electron.* **8** 823–832
[3] Tanaka S, Iwai S and Aoyagi Y 1996 *Appl. Phys. Lett.* **69** 4096–4098

[4] Widmann F, Simon J, Daudin B, Feuillet G, Rouvière J L, Pelekanos N T and Fishman G 1998 *Phys. Rev. B* **58** R15989–R15992
[5] Daudin B, Widmann F, Feuillet G, Samson Y, Arlery M and Rouviére J L 1997 *Phys. Rev. B* **56** R7069–R7072
[6] DeRinaldis S, D'Amico I, Biolatti E, Rinaldi R, Cingolani R and Rossi F 2002 *Phys. Rev. B* **65** 081309(R)
[7] Krummheuer B, Axt V M, Kuhn T, D'Amico I and Rossi F 2005 *Phys. Rev. B* **71** 235329
[8] Heber J D, Gmachl C, Ng H M and Cho A Y 2002 *Appl. Phys. Lett.* **81** 1237–1239
[9] Iizuka N, Kaneko K, Suzuki N, Asano T, Noda S and Wada O 2000 *Appl. Phys. Lett.* **77** 648–650
[10] Moumanis K, Helman A, Fossard F, Tchernycheva M, Lusson A, Julien F H, Damilano B, Grandjean N and Massies J 2003 *Appl. Phys. Lett.* **82** 868–870
[11] Tchernycheva M, Nevou L, Doyennette L, Helman A, Colombelli R, Julien F H, Guillot F, Monroy E, Shibata T and Tanaka M 2005 *Appl. Phys. Lett.* **87** 101912
[12] Jovanović V D, Indjin D, Ikonić Z and Harrison P 2004 *Appl. Phys. Lett.* **84** 2995–2997
[13] Vukmirović N, Jovanović V D, Indjin D, Ikonić Z, Harrison P and Milanović V 2005 *J. Appl. Phys.* **97** 103106
[14] Andreev A D and O'Reilly E P 2000 *Phys. Rev. B* **62** 15851–15870
[15] Ranjan V, Allan G, Priester C and Delerue C 2003 *Phys. Rev. B* **68** 115305
[16] Baer N, Schulz S, Schumacher S, Gartner P, Czycholl G and Jahnke F 2005 *Appl. Phys. Lett.* **87** 231114
[17] Bagga A, Chattopadhyay P K and Ghosh S 2003 *Phys. Rev. B* **68** 155331
[18] Bagga A, Chattopadhyay P K and Ghosh S 2005 *Phys. Rev. B* **71** 115327
[19] Fonoberov V A and Balandin A A 2003 *J. Appl. Phys.* **94** 7178–7186
[20] Vukmirović N, Indjin D, Jovanović V D, Ikonić Z and Harrison P 2005 *Phys. Rev. B* **72** 075356
[21] Tronc P, Smirnov V P and Zhuravlev K S 2004 *Phys. Status Solidi B* **241** 2938–2947
[22] Berkowicz E, Gershoni D, Bahir G, Lakin E, Shilo D, Zolotoyabko E, Abare A C, Denbaars S P and Coldren L A 2000 *Phys. Rev. B* **61** 10994–11008
[23] Vurgaftman I and Meyer J R 2003 *J. Appl. Phys.* **94** 3675–3696
[24] Fiorentini V, Bernardini F, DellaSala F, DiCarlo A and Lugli P 1999 *Phys. Rev. B* **60** 8849–8858
[25] Baraff G A and Gershoni D 1991 *Phys. Rev. B* **43** 4011–4022
[26] Gershoni D, Brener I, Baraff G A, Chu S N G, Pfeiffer L N and West K 1991 *Phys. Rev. B* **44** 1930–1933
[27] Gershoni D, Henry C H and Baraff G A 1993 *IEEE J. Quantum Electron.* **29** 2433–2450
[28] Li S S, Xia J B, Yuan Z L, Xu Z Y, Ge W, Wang X R, Wang Y, Wang J and Chang L L 1996 *Phys. Rev. B* **54** 11575–11581
[29] Harrison P 2005 *Quantum Wells, Wires and Dots, 2nd edition* (John Wiley and Sons Ltd., Chichester, England)
[30] Li S S, Chang K and Xia J B 2005 *Phys. Rev. B* **71** 155301
[31] Williams D P, Andreev A D, O'Reilly E P and Faux D A 2005 *Phys. Rev. B* **72** 235318
[32] Ikonić Z, Milanović V and Tadić M 1995 *J. Phys.: Condens. Matter* **7** 7045–7052
[33] Vukmirović N, Ikonić Z, Jovanović V D, Indjin D and Harrison P 2005 *IEEE J. Quantum Electron.* **41** 1361–1368
[34] Bester G and Zunger A 2005 *Phys. Rev. B* **71** 045318
[35] Milošević I, Stevanović V, Tronc P and Damnjanović M 2006 *J. Phys.: Condens. Matter* **18** 1939–1953
[36] Stier O, Grundmann M and Bimberg D 1999 *Phys. Rev. B* **59** 5688–5701
[37] Elliott J P and Dawber P G 1979 *Symmetry in Physics* (Macmillan, London)
[38] Andreev A D and O'Reilly E P 2001 *Appl. Phys. Lett.* **79** 521–523